



Improvement of photocatalytic decomposition of methyl orange by modified MWCNTs, prediction of degradation rate using statistical models

Sedigheh Abbasi^{1,*}

¹ Central Research Laboratory, Esfarayen University of Technology, Esfarayen, North Khorasan, Iran

Received: 25 January 2021

Accepted: 6 March 2021

Published online:
26 May 2021

© The Author(s), under exclusive licence to Springer Science+Business Media, LLC, part of Springer Nature 2021

ABSTRACT

Multi-walled carbon nanotubes (MWCNTs) have been successfully modified with TiO₂ nanoparticles via a two-step hydrolysis technique. Firstly, the pristine MWCNTs are functionalized in nitric acid (HNO₃) to creation of oxygen containing groups. Secondly, TiO₂ nanoparticles are synthesized on the surface of functionalized MWCNTs through hydrolysis method. The synthesized samples have been used as photocatalyst for decomposition of methyl orange (MO) as dye organic pollutant. The characterization of samples using X-ray diffraction pattern (XRD) confirm the presence of TiO₂ nanoparticles with mixture of anatase and rutile phases. Regarding the photocatalytic performance of TiO₂ nanoparticles and modified MWCNTs with TiO₂ nanoparticles, it observed that the degradation rate of MO increases by increasing the irradiation time from 5 to 35 min. The variation of degradation rate upon pH of suspension reveals that the maximum and minimum degradation rate are in acidic (pH = 3) and neutral condition (pH = 7). Meanwhile, the results show that the presence of MWCNTs leads to the enhancement of degradation rate. The analysis of variance (ANOVA) results confirm that both of main factors (irradiation time and pH) and their interaction have a significant influence on the degradation rate of MO. However, the effect of irradiation time is more than that of pH and their interaction. The graphical methods verify the quality and adequacy of the statistical models for prediction of the degradation rate.

1 Introduction

The elimination of organic contaminates from wastewater of industries is a major problem in the recent decades. The application of semiconductor photocatalysts is a new approach for decomposition

of organic pollutants [1, 2]. In this technique, a light source with energy higher than the bandgap of used semiconductors is applied [3]. The irradiation of the semiconductors leads to the migration of electrons that are located in the valence band to the conduction band [4–6]. The transmittance of electrons causes the

Address correspondence to E-mail: s.abbasi@esfarayen.ac.ir; abasi_1362@yahoo.com

formation of electrons and holes in the valence band and conduction layer, respectively [1, 7]. The formed electrons and holes are able to react by water and oxygen. The reaction among them causes the creation of different kinds of radical species that can act as decomposer of organic molecules [8, 9]. The recombination of the formed electrons and holes can restrict the removal efficiency of pollutants. Therefore, the photocatalytic performance of the semiconductor photocatalysts depends on the separation efficiency of produced charges [10]. According to the previous reports, there are several methods that can be applied for the decreasing of recombination rate of produced charges. For example, the doping of materials that can act as electron sinks (such as Ag and Au) on the surface of photocatalysts [11, 12]. The other technique for decreasing the recombination rate of electrons and holes is application of a specific support with high surface area such as multi-walled carbon nanotubes (MWCNTs) and graphene oxide (GO) [13]. The synthesis of photocatalysts on the surface of these materials as template can significantly enhance the photocatalytic performance. It can be attributed to the effect of MWCNTs and GO on the migration rate of electrons from valence band [14, 15]. The coupling of semiconductor oxides to the carbon supports can decrease the recombination of electrons and holes. Meanwhile, it has a synergistic effect on the enhancement of energy range that stimulates electrons [16]. Among the most widely used semiconductor photocatalysts, TiO_2 has been received great attention due to its excellent photocatalytic performance, environmental compatibility, low cost and wide bandgap [17–21]. In the recent years, several coupled photocatalysts such as GO–ZnO [22], CNT–ZnO [7, 9, 23], Fe_3O_4 –GO–ZnO [15], CNT– TiO_2 [2] and SnO_2 –CNT [16] report the augmentation of photocatalytic activity for degradation of numerous organic pollutants. Despite extensive research on the removal of numerous organic pollutants, no statistical study of the impact of acidity on the removal of dye organic pollutants has been performed using modified MWCNTs with TiO_2 .

The main purpose of this research is synthesis of TiO_2 nanoparticles and coupled of MWCNTs– TiO_2 as photocatalyst for degradation of methyl orange (MO). The synthesized photocatalysts are characterized by means of X-ray diffraction pattern (XRD) using Bruker D8 Advance. The influence of experimental factors such as illumination time and pH of suspension

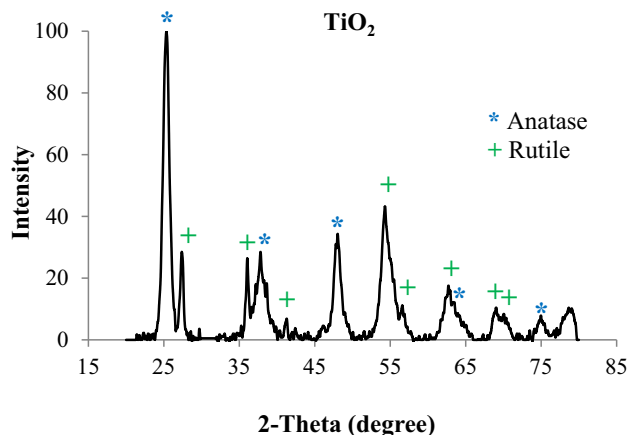


Fig. 1 XRD pattern of TiO_2 nanoparticles

are investigated on the photocatalytic performance of the samples. The experimental results are analyzed based on the analysis of variance (ANOVA) and response surface methodology (RSM). The influence of main factors and their interaction on the degradation rate of MO are studied. Finally, the adequacy of the presented statistical models for the prediction of degradation rate is investigated based on the graphical method.

2 Experimental

2.1 Chemicals

MWCNTs with average diameter about 40–60 nm and length 5–15 μm are purchased as support material. Nitric acid (HNO_3 , 65%, Merck), Tetrachloride titanium (TiCl_4 , 99%, Merck) and Methyl orange (99.5%, Merck) with analytical grade are applied without any purification. All of aqueous suspensions are based on distilled water. Hydrochloric acid (HCl, 99%, Merck) and sodium hydroxide (NaOH, 99%, Merck) are used to adjust the pH of the suspensions.

2.2 Preparation of photocatalysts

Synthesis procedure of TiO_2 nanoparticles as applied photocatalysts is same as method that is described in our previous reports [24, 25]. The preparation of modified MWCNTs with TiO_2 nanoparticles consists of two steps including functionalization of MWCNTs and surface decoration with TiO_2 nanoparticles. The functionalization step is performed using acid-treatment process. For this purpose, 0.1 g of the as-

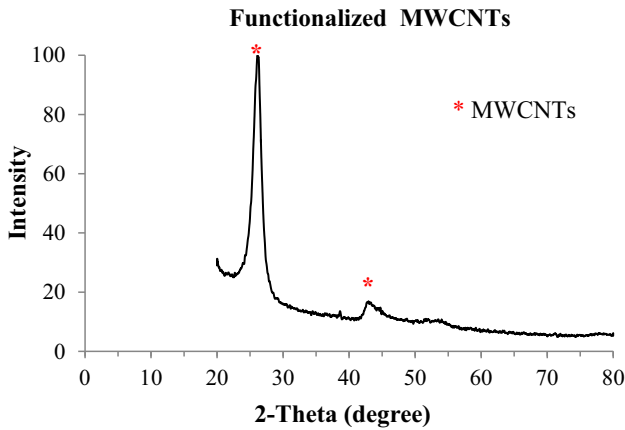


Fig. 2 XRD pattern of functionalized MWCNTs

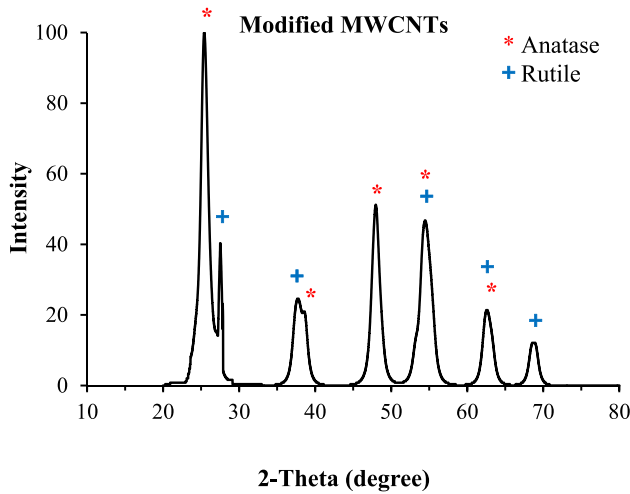


Fig. 3 XRD pattern of modified MWCNTs with TiO₂ nanoparticles

received MWCNTs is dispersed in 50 ml of HNO₃ and is agitated for 120 min using a magnetic stirrer. Then the suspension is transferred to an ultrasonic bath and the treatment process is continues for 120 min. Finally, the treated MWCNTs are filtered, washed and dried at 80 °C for an overnight. The second step is based on the hydrolysis method to synthesis of TiO₂ nanoparticles on the surface of the prepared functionalized MWCNTs. 0.04 g of dried acid treated MWCNTs is dispersed in 100 ml of distilled water and is agitated for 30 min. Then, 0.4 ml of TiCl₄ is added to the mixture at room temperature and mixed for about 5 h. Subsequently, the temperature of mixture is raised to 65 °C and maintained for 12 h. Finally, the mixture is filtered and washed. The prepared dried powder is calcined at 350 °C for 3 h.

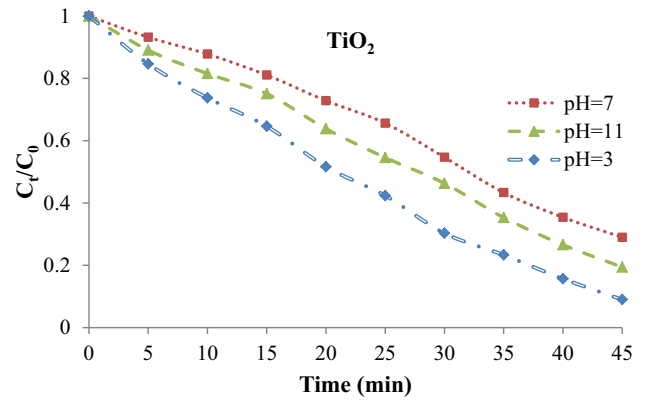


Fig. 4 Variation of MO concentration with respect to the irradiation time and pH using TiO₂ nanoparticles as photocatalyst

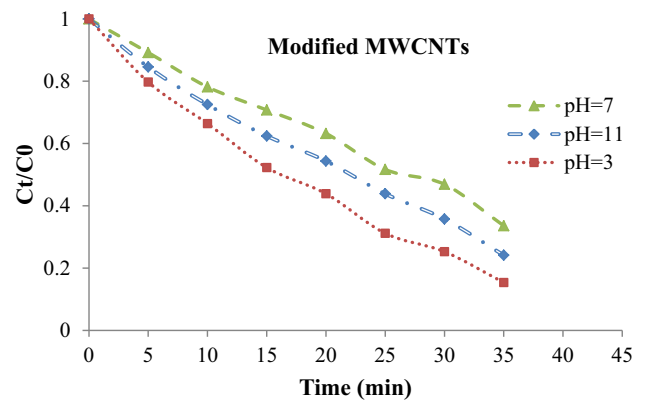


Fig. 5 Variation of MO concentration with respect to the irradiation time and pH using modified MWCNTs with TiO₂ as photocatalyst

2.3 Experimental procedure for photocatalytic decomposition of MO

The photocatalytic experiments for decomposition of MO are carried out in a batch reactor in three pH (pH = 3, pH = 7 and pH = 11). The temperature of the suspension in the reactor is controlled using circulation of water. The MO suspension (10 mg/ml) is located at a dark chamber for 60 min. Then, the initial concentration of MO (C_0) that is attributed to the initial adsorption intensity (A_0) is recorded by means of a Lambda EZ 201 spectrophotometer (Perkin Elmer Company). The suspension is irradiated using a UV lamp (150 W). Every 5 min, some of suspension is discharged and filtered. The remained concentration of MO (C_t) in the suspension can be evaluated by recording the adsorption at each interval (A_t). The degradation rate of pollutant can be expressed by

C_t/C_0 . The statistical investigations based on the analysis of variance (ANOVA) are performed using design of experiment (DOE).

3 Results and discussion

3.1 XRD analysis

The XRD pattern of the synthesized TiO_2 nanoparticles is illustrated in Fig. 1 for investigation of crystal structure. Based on this Figure, it can be observed that the synthesized TiO_2 nanoparticles have two main phases such as anatase and rutile. The diffraction peaks that are referred to the anatase phase and rutile phase are labeled using different symbols. So that, the observed sharp characteristic peaks that is located at $2\theta=25.35^\circ, 37.96^\circ, 48.02^\circ, 62.89^\circ$ and 75.20° are assigned to the (101), (004), (200), (204) and (215) crystal orientations of the anatase phase of synthesized titania [26, 27]. The diffraction peaks at $27.33^\circ, 36.26^\circ, 41.36^\circ, 54.39^\circ, 56.66^\circ, 62.26^\circ, 68.98^\circ$ and 70.11° belong to the (110), (101), (111), (211), (220), (002), (301) and (112) planes of TiO_2 nanoparticles with rutile crystal structure. Therefore, the both of crystal structures (anatase and rutile) can be confirmed in the synthesized TiO_2 nanoparticles. The fraction of each crystal structures can be approximately calculated using Eq. (1) [28, 29]:

$$\%A = \frac{I_A}{I_A + 1.265I_R} \times 100 \quad (1)$$

where A is the amount of titania with anatase crystal structure. I_A and I_R are corresponded to the intensity of the main characteristic peaks of anatase (101) and rutile (211) phases, respectively. Therefore, according to this equation the amount of anatase and rutile crystal structures are about to 63 and 37%, respectively.

The XRD pattern of functionalized MWCNTs using nitric acid is presented in Fig. 2. The main characteristic peaks of MWCNTs that is belonged to the (002) and (100) Bragg reflection planes of graphite can be detected at 26.31° and 42.76° , respectively [28, 30]. Figure 3 illustrates the XRD pattern of the modified MWCNTs with TiO_2 nanoparticles. This Figure suggests the formation of the both phases of anatase and rutile crystallites. As can be seen, the major peaks of the synthesized MWCNTs– TiO_2 are located at about $25.33^\circ, 27.16^\circ, 36.14^\circ, 37.85^\circ, 47.95^\circ, 54.16^\circ, 62.35^\circ$ and

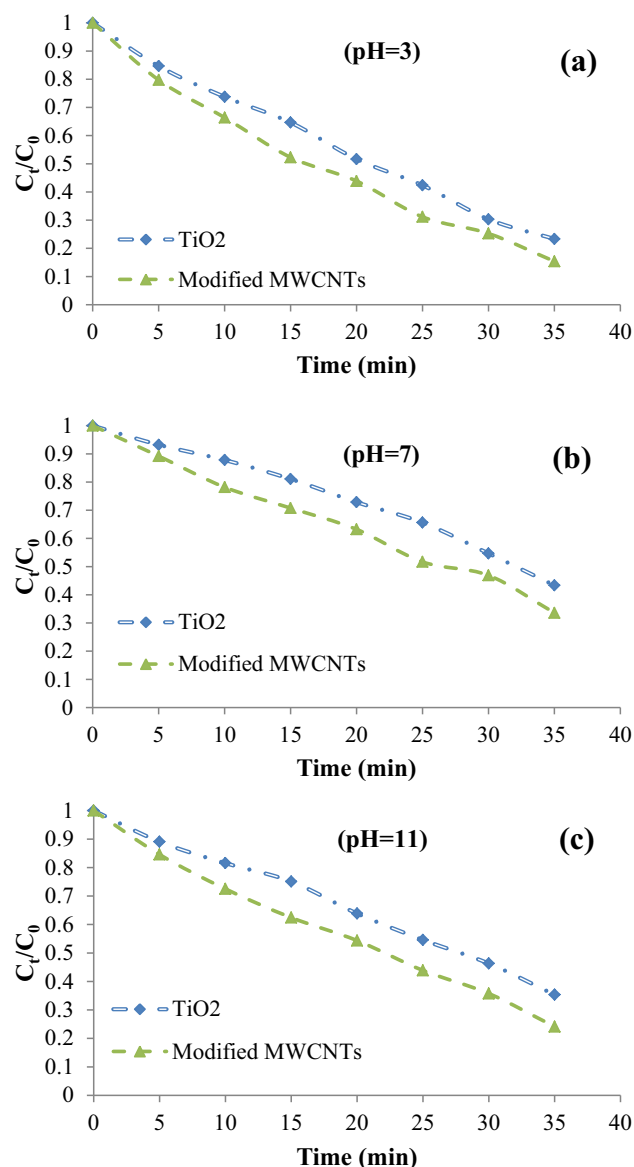


Fig. 6 Comparison between variation of MO concentration with respect to the irradiation time using TiO_2 nanoparticles and modified MWCNTs at different pH, **a** pH = 3, **b** pH = 7, **c** pH = 11

68.51° . The observed diffraction peaks at $25.33^\circ, 37.85^\circ, 47.95^\circ, 54.16^\circ$ and 62.35° are corresponded to the (101), (004), (200), (105) and (204) crystal facets of anatase TiO_2 , respectively [17]. Meanwhile, the located peaks at $27.16^\circ, 36.14^\circ, 54.16^\circ, 62.35^\circ$ and 68.51° are indexed to the (110), (101), (211), (002) and (301) planes of rutile TiO_2 , respectively [25]. The main characteristic peaks of MWCNTs are not detectable in the XRD pattern of the modified MWCNTs with TiO_2 . It can be due to the overlap of diffraction peak

Table 1 Analysis of variance for MO degradation rate using TiO₂ nanoparticles

Source	Sum of square	Df	Mean squares	F value	P value	% Contribution	
Model	2.83	20	0.14	1598.45	< 0.0001	–	Significant
A (time)	2.64	6	0.44	4981.66	< 0.0001	93.37	Significant
B (pH)	0.17	2	0.087	979.27	< 0.0001	6.12	Significant
AB	0.011	12	8.872E–04	10.03	< 0.0001	0.38	Significant
Lack of fit	0	0	–	–	–	0.000	Not significant
Pure error	3.71E–03	42	8.843E–05	–	–	0.13	–
Total	2.34	62	–	–	–	–	–

Table 2 Analysis of variance for MO degradation rate using modified MWCNTs with TiO₂ nanoparticles

Source	Sum of square	Df	Mean squares	F value	P value	% Contribution	
Model	3.07	20	0.15	3232.53	< 0.0001	–	Significant
A (time)	2.92	6	0.49	10,254.87	< 0.0001	95.11	Significant
B (pH)	0.14	2	0.071	1495.84	< 0.0001	4.62	Significant
AB	6.15E–03	12	5.12E–04	10.80	< 0.0001	0.20	Significant
Lack of fit	0	0	–	–	–	0.000	Not significant
Pure error	1.99E–03	42	4.74E–05	–	–	0.065	–
Total	3.07	62	–	–	–	–	–

of (002) plane of MWCNTs which is located at 26.11° and sharp peak of (101) plane of anatase TiO₂.

3.2 The study of MO degradation rate

Figures 4 and 5 show the variation of MO concentration with respect to the irradiation time and pH using TiO₂ nanoparticles and modified MWCNTs, respectively. Given the trend of concentration changes, it can be observed that the ratio of final to initial concentration of MO decreases by increasing of UV irradiation time (this behavior is the same at all of the studied pH). The main reason for the decrease in pollutant concentration over time is the amount of created electron–hole pairs. When the photocatalysts are exposed to the UV radiation, the electrons in the valence layer are excited. The excitation of electrons causes the electrons to move from the valence layer to the conduction layer [24, 31]. Electron displacement causes the formation of electrons and holes in the valence layer and conduction layer, respectively. The formed electron–hole pairs can react with water and dissolved oxygen in the suspension containing pollutants and produce the oxidizing radicals such as OH• and O₂•, respectively. These types of oxidizing radicals can successfully degrade and decompose the

organic pollutants. Therefore, the decomposer radicals can be enhanced with increasing the irradiation time [14, 32]. The results of the effect of PH on methyl orange concentration show that the acidic medium have the greatest effect on the removal of pollutant. However, in neutral medium the rate of degradation of methyl orange is lower than that of acidic and alkaline conditions. The high rate of decomposition of methyl orange in the acidic medium is attributed to the presence of hydrogen ions (H⁺). The H⁺ ions in the suspension can react with the produced electrons (e⁻) and form the hydrogen radicals (H•). Finally, the derived radicals can adsorb the oxygen of the solution and produce the OH• [17, 33]. Therefore, it can be deduced that as the number of hydrogen ions (in acidic medium) increases, the number of decomposing radicals also increases. The efficiency of MO removal using a photocatalyst is affected by the surface charge of the photocatalyst. This is because as the surface charge of the photocatalyst increases, the dispersion of the photocatalyst in the suspension increases. Therefore, a higher level of photocatalyst is exposed to the UV radiation. This increases the amount of electron excitation and oxidizing radicals. Therefore, due to the reduction of the surface charge of the photocatalyst under neutral conditions (pH =

7), the removal rate of the MO under neutral conditions is less than the acidic and alkaline conditions [34].

Figure 6 illustrates the comparison between variation of MO concentration with respect to the irradiation time using TiO₂ nanoparticles and modified MWCNTs at different pH. The presented results show that the concentration of methyl orange at each time point of irradiation and all three pH when using modified MWCNTs is lower than TiO₂ nanoparticles. Therefore, these results can confirm the positive effect of carbon nanotubes on methyl orange removal. The main role of carbon nanotubes is to reduce the agglomeration rate of TiO₂ nanoparticles. Therefore, a higher level of photocatalyst can be exposed to the UV radiation [35, 36]. This causes the increasing of excitation electrons of valence band in the modified MWCNTs with TiO₂ nanoparticles photocatalyst. The enhancement of the excited electrons leads to the increasing of transmitted electrons from valence band to the conduction band. Therefore, more hydroxyl radicals are produced in the suspension containing modified MWCNTs as photocatalyst.

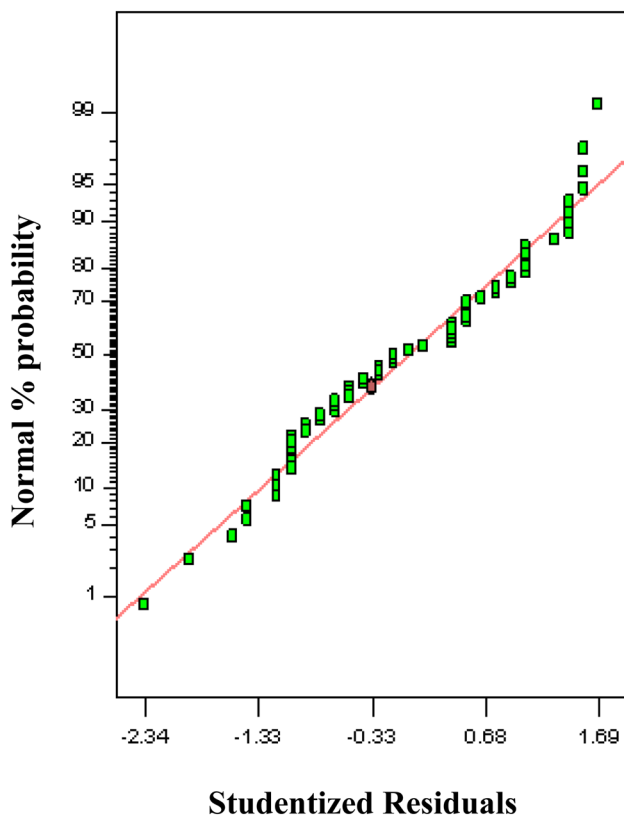


Fig. 7 Normal plot of residuals for degradation rate of MO using TiO₂ nanoparticles

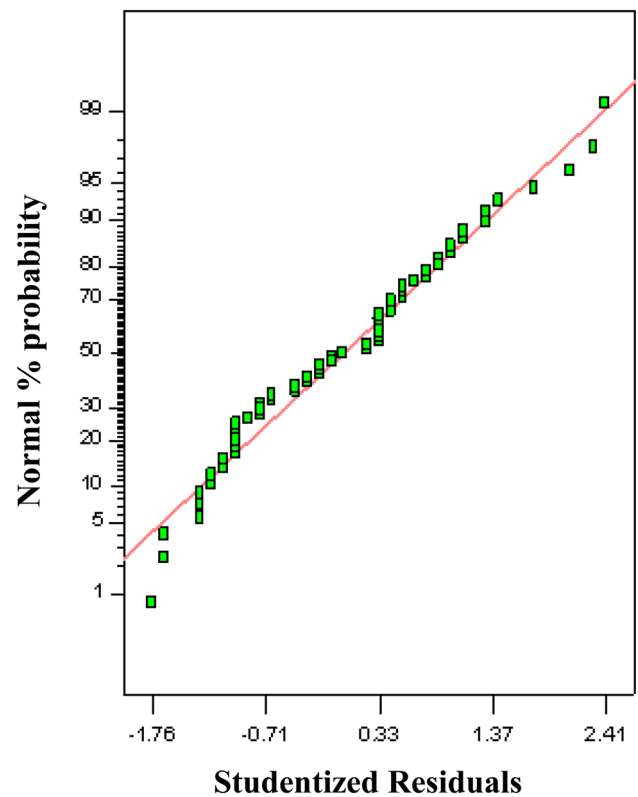


Fig. 8 Normal plot of residuals for degradation rate of MO using modified MWCNTs with TiO₂ nanoparticles

Thus it can be confirmed that the removal rate of methyl orange by modified MWCNTs is substantially higher than TiO₂ nanoparticles.

3.3 The analysis of variance study

Tables 1 and 2 present the results of analysis of variance for MO degradation rate using TiO₂ nanoparticles and modified MWCNTs with TiO₂ nanoparticles, respectively. It can be seen that the degree of freedom (*Df*) for factor *A* (irradiation time) and factor *B* (pH) is equal to 6 and 2, respectively. Thus, the number of factor's levels of *A* and *B* is 7 (5, 10, 15, 20, 25, 30 and 35 min) and 3 (pH = 3, pH = 7 and pH = 11), respectively. The *Df* value for interaction between *A* and *B* (*AB*) is the *Df* multiple of single factors. The importance of each single factor and their interactions can be evaluated using *F* value and *P* value. The significant parameters have the sum of square value more than error. Therefore, it can be deduced that the enhancement of *F* value leads to the increasing of factor's importance [37, 38]. According to the *F* values of presented factors in Tables 1 and 2, it can be observed that all of the

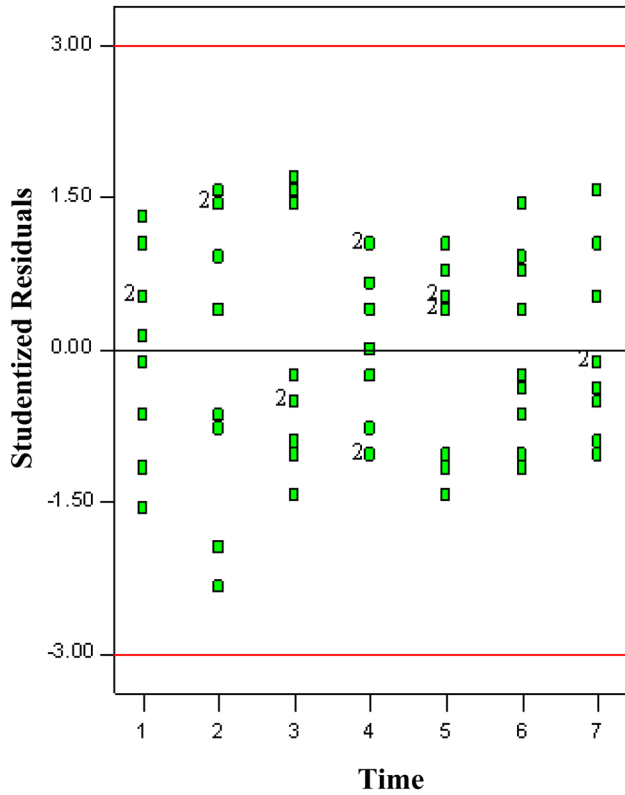


Fig. 9 Plot of studentized residual versus time of irradiation in suspension containing TiO₂ nanoparticles

parameters have reasonable *F* value. It means that both of main factors and their interaction have significant effect on the degradation rate of MO. According to the results of *F* value, it can be concluded that the variation of the factors' levels can reasonably vary the degradation rate of MO. Based on the results of these Tables, it is clear that the *F* value of factor A for degradation rate of MO using TiO₂ nanoparticles and modified MWCNTs are 4981.66 and 10,254.87, respectively. However, the *F* value of factor B in Tables 1 and 2 is 979.27 and 1495.84, respectively. The comparison between *F* values of factor A and factor B represents that irradiation time have *F* value more than pH. Meanwhile, as can be shown, the contribution percent of factor A on the MO degradation rate using TiO₂ nanoparticles and modified MWCNTs is 93.37 and 95.11, respectively. In addition, 6.12 and 4.62% of degradation rate of MO can be affected by pH of suspension containing TiO₂ nanoparticles and modified MWCNTs, respectively. It shows that the influence of irradiation time on the degradation of MO is more than that of pH. It may be due to the effect of irradiation time on

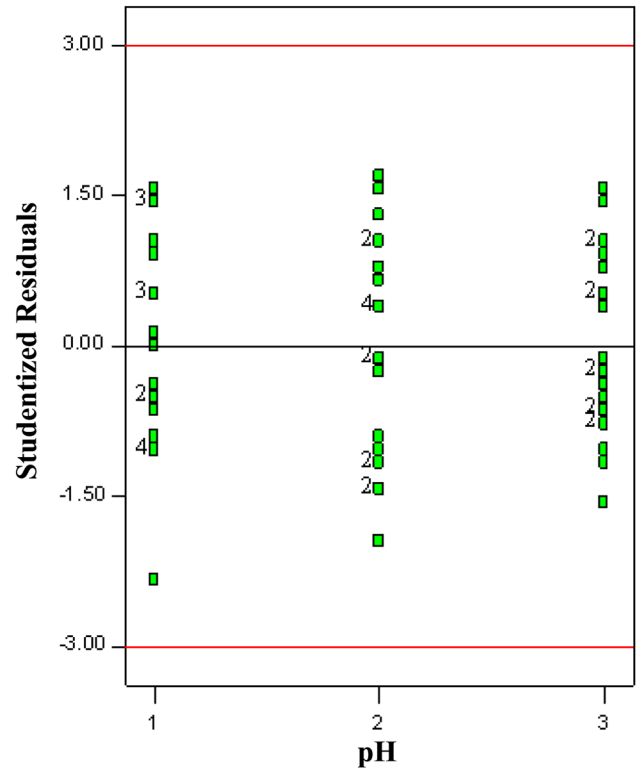


Fig. 10 Plot of studentized residual versus pH in suspension containing TiO₂ nanoparticles

the created electron hole pairs. Besides the *F* value of factors, the significant factors can be distinguished based on the *P* value. So that, each factor that have *P* value less than the significance level ($\alpha = 0.05$) is assigned as a significant factor [39]. The results of Tables 1 and 2 confirm that irradiation time, pH and their interaction have *P* value less than 0.05. Therefore, all of these parameters are assigned as significant factors. Therefore, there is not any insignificant factor. The results of Tables 1 and 2 also confirm it. As can be observed, the *Df* and sum of square of lack of fit is zero. The lack of fit contain the insignificant parameters [40]. Therefore, it can be concluded that the proposed models in Tables 1 and 2 involve only the significant factors. Thus the presented statistical models can accurately predict the variation of MO degradation rate with respect to the irradiation time, pH and their interaction.

However, the quality of the both proposed models is justified by ANOVA tables; the assumptions that are applied for the application of ANOVA should be verified. The analysis of residuals based on the graphical technique is common for validation of degradation rate models of TiO₂ nanoparticles and

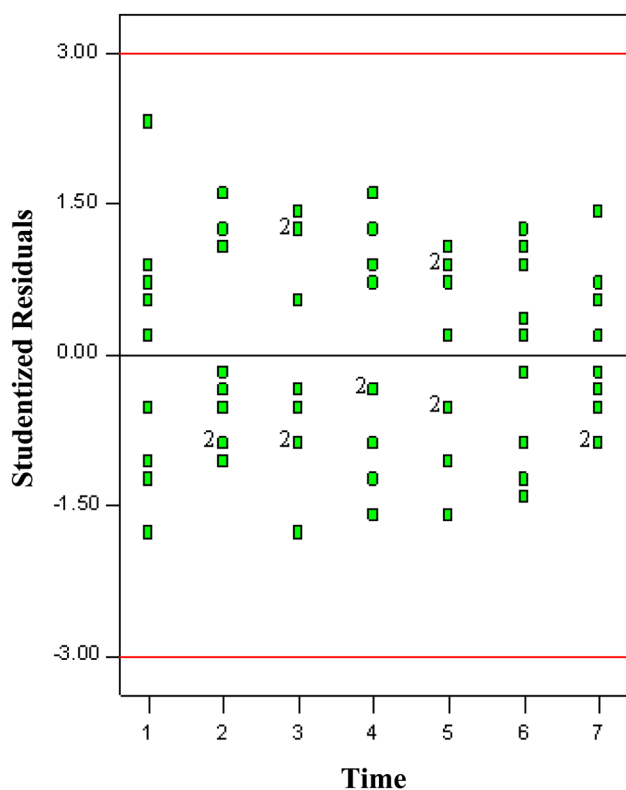


Fig. 11 Plot of studentized residual versus time of irradiation in suspension containing modified MWCNTs with TiO_2 nanoparticles

modified MWCNTs. The graphical approach can show the relationship between factors and response. In this method, the residuals are converted to the studentized residuals and are plotted versus main factors, run number or on normal probability [40, 41]. The first assumption of the ANOVA is the normality of error that can be verified using normal probability plot. Figures 7 and 8 illustrate the normal plot of residuals for degradation rate of MO using TiO_2 nanoparticles and modified MWCNTs, respectively. The patterned distribution of studentized residuals around mean zero in Figs. 7 and 8 reveals the normality of errors for TiO_2 nanoparticles and modified MWCNTs models. Thus, the degradation rate transformation is not required. Therefore, it can be deduced that both of the models can accurately fit the experimental degradation rates.

The second assumption in the ANOVA method is the independently distribution of error and constant variance of all studied factors and their levels [40]. The verification of this assumption can be carried out using the plotting of studentized residuals versus independent factors (such as irradiation time and pH

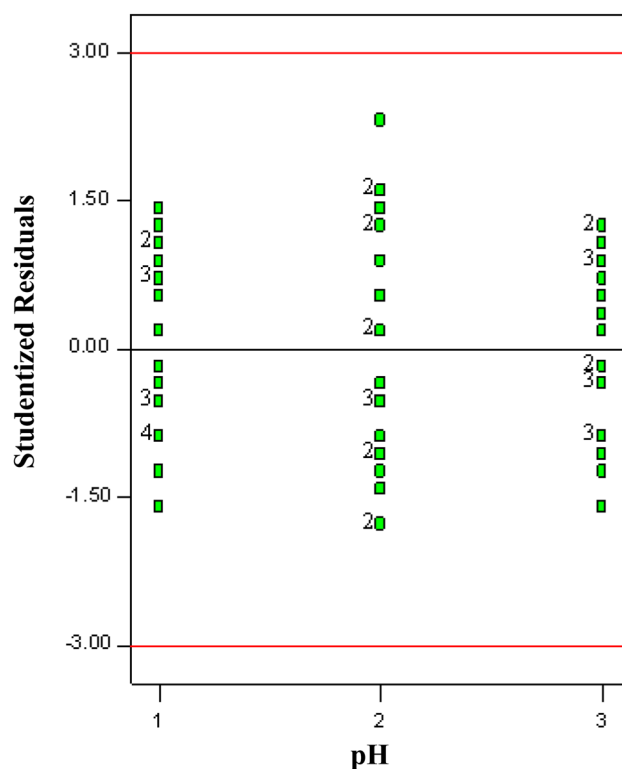


Fig. 12 Plot of studentized residual versus pH in suspension containing modified MWCNTs with TiO_2 nanoparticles

of suspension), run number and predicted responses values that are estimated by model. The studentized residual plot versus time of irradiation and pH of suspension containing TiO_2 nanoparticles are shown in Figs. 9 and 10, respectively. It is clear that all of the design points are located in the range of -3 and 3 . Therefore, it can be confirmed that there is not any outlier and discrepancy in design point of TiO_2 nanoparticles. The same results can be observed in Figs. 11 and 12 for studentized residual plot versus time of irradiation and pH of suspension containing modified MWCNTs with TiO_2 nanoparticles. Therefore, these results can verify the adequacy of the both statistical models for estimation of MO degradation rate with respect to the irradiation time and pH.

The correlation between experimental data and predicted values that are obtained by statistical model of TiO_2 nanoparticles and modified MWCNTs with TiO_2 nanoparticles are presented in Figs. 13 and 14, respectively. Regarding these Figures, it can be observed that there is a good consistency among actuals and predicted degradation rate of MO. Therefore, the adequacy of the both models for estimation of the degradation rate can be confirmed.

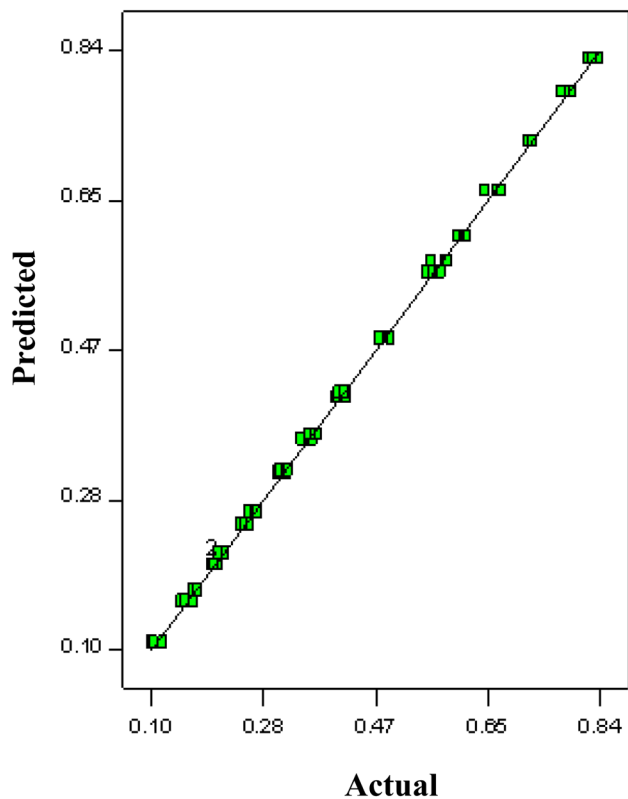


Fig. 13 Predicted versus actual value of MO degradation rate using TiO_2 nanoparticles

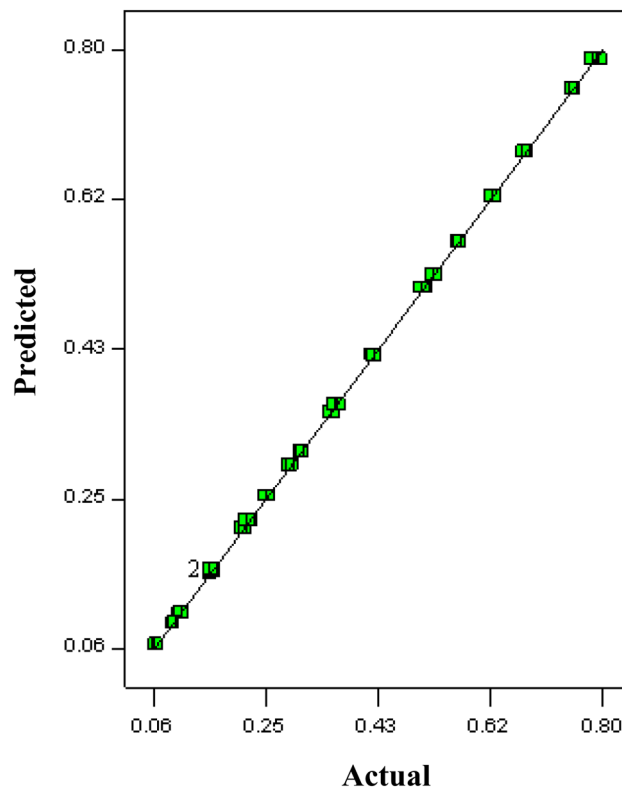


Fig. 14 Predicted versus actual value of MO degradation rate using modified MWCNTs with TiO_2 nanoparticles

3.4 The analysis of MO degradation rate based on response surface methodology

The response surface method (RSM) is a three-dimensional approach for investigation of the response variation upon simultaneous influence of two factors [37]. Figures 15 and 16 illustrate the response surface of MO degradation rate using TiO_2 nanoparticles and modified MWCNTs with TiO_2 nanoparticles, respectively. These two Figures show that the degradation rate of MO using both of photocatalysts increases by enhancement of irradiation time up to 35 min. Regarding the influence of pH on MO degradation rate using TiO_2 nanoparticles and modified MWCNTs, it is clear that the maximum and minimum degradation rate is attributed to the suspension with $\text{pH} = 3$ and $\text{pH} = 7$. It means that at the same time of irradiation, the concentration of MO in the suspension with acidic condition ($\text{pH} = 3$) is lower than that of neutral condition ($\text{pH} = 7$). Based on the slope of these two curves, it can be observed that the variation of MO concentration with respect to the

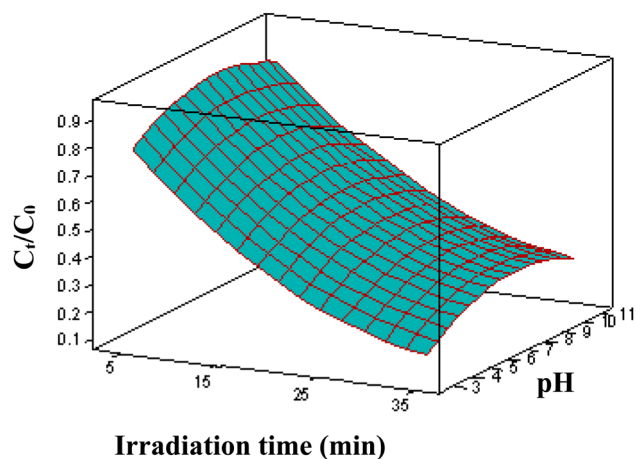


Fig. 15 Response surface of MO degradation rate using TiO_2 nanoparticles

irradiation time is more than that of pH. Therefore, it can be deduced that the influence of irradiation time is more than pH. The same results is observed in ANOVA.

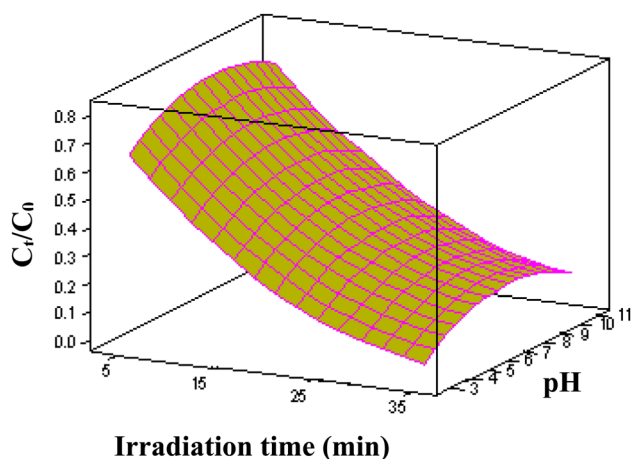


Fig. 16 Response surface of MO degradation rate using MWCNTs with TiO₂ nanoparticles

4 Conclusions

TiO₂ nanoparticles and modified MWCNTs are prepared via hydrolysis method. The XRD patterns of the as-prepared samples show that the structure of TiO₂ nanoparticles is anatase and rutile. The comparison between degradation rates of MO using synthesized photocatalysts reveals that the modified MWCNTs have higher photocatalytic performance rather than TiO₂ nanoparticles. The investigation of degradation rate based on the ANOVA show that the variation of level of each factor could significantly change the response. Meanwhile, at 5% level of probability, the proposed models are significant. So that, the graphical results show that there is a good consistency among actuals and predicted values of degradation rate of MO using the models. The response surface method validates the ANOVA results.

Acknowledgements

We are thankful from boss of central research laboratory of Esfarayen University of Technology.

Declarations

Conflict of interest We declare that we have no financial and personal relationships with other people or organization that can inappropriately influence our work.

References

1. N. Bouazza, M. Ouzzine, M.A.L.-R. Denas, D. Eder, A. Linares-Solano, TiO₂ nanotubes and CNT–TiO₂ hybrid materials for the photocatalytic oxidation of propene at low concentration. *Appl. Catal. B* **92**, 377–383 (2009)
2. Y. Dong, D. Tang, C. Li, Photocatalytic oxidation of methyl orange in waterphase by immobilized TiO₂–carbon nanotube nanocomposite photocatalyst. *Appl. Surf. Sci.* **296**, 1–7 (2014)
3. S. Abbasi, M.-S. Ekrami-Kakhki, M. Tahari, Modeling and predicting the photodecomposition of methylene blue via ZnO–SnO₂ hybrids using design of experiments (DOE). *J. Mater. Sci.* **28**, 15306–15312 (2017)
4. X.-T. Yin, J. Li, D. Dastan, W.-D. Zhou, H. Garmestani, F.M. Alamgir, Ultra-high selectivity of H₂ over CO with a p-n nanojunction based gas sensors and its mechanism. *Sens. Actuators* **319**, 128330 (2020)
5. K. Shan, F. Zhai, Z. Yi, X. Yin, D. Dastan, F. Tajabadi, A. Jafari, S. Abbasi, Mixed conductivity and the Conduction Mechanism Of The Orthorhombic CaZrO₃ based materials. *Surf. Interfaces* **23**, 100905 (2021)
6. K. Shan, Z. Yi, X. Yin, D. Dastan, H. Garmestani, Y-doped CaZrO₃/Co₃O₄ as novel dense diffusion barrier materials for limiting current oxygen sensor. *Dalton Trans.* **49**, 8549–8556 (2020)
7. G. Zhu, H. Wang, G. Yang, L. Chen, P. Guo, L. Zhang, A facile synthesis of ZnO/CNTs hierarchical microsphere composites with enhanced photocatalytic degradation of methylene blue. *RSC Adv.* **5**, 2476–72481 (2015)
8. A. Ghaderi, S. Abbasi, F. Farahbod, Synthesis, characterization and photocatalytic performance of modified ZnO nanoparticles with SnO₂ nanoparticles. *Mater. Res. Express* **5**, 065908 (2018)
9. N. Roozban, S. Abbasi, M. Ghazizadeh, The experimental and statistical investigation of the photo degradation of methyl orange using modified MWCNTs with different amount of ZnO nanoparticles. *J. Mater. Sci.* **28**, 7343–7352 (2017)
10. A. Ghaderi, S. Abbasi, F. Farahbod, Synthesis of SnO₂ and ZnO nanoparticles and SnO₂–ZnO hybrid for the photocatalytic oxidation of methyl orange. *Iran. J. Chem. Eng.* **12**, 96–105 (2015)
11. H. Wang, S. Baek, J. Lee, S. Lim, High photocatalytic activity of silver-loaded ZnO–SnO₂ coupled catalysts. *Chem. Eng. J.* **146**, 355–361 (2009)
12. N. Zhou, L. Polavarapu, N. Gao, Y. Pan, P. Yuan, Q. Wang, Q.-H. Xu, TiO₂ coated Au/Ag nanorods with enhanced photocatalytic activity under visible light irradiation. *Nanoscale* **5**, 4236–4241 (2013)

13. S. Abbasi, M. Hasanpour, M.S.E. Kakhki, Removal efficiency optimization of organic pollutant (methylene blue) with modified multi-walled carbon nanotubes using design of experiments (DOE). *J. Mater. Sci.* **28**, 9900–9910 (2017)
14. S. Abbasi, Investigation the kinetic reaction variation of the methyl orange decomposition using decorated multi-walled carbon nanotubes with ZnO nanoparticles, influence of nanoparticle content. *J. Environ. Health Eng.* **5**, 113–122 (2018)
15. S. Abbasi, F. Ahmadpoor, M. Imani, M.-S. Ekrami-Kakhki, Synthesis of magnetic Fe₃O₄@ZnO@graphene oxide nanocomposite for photodegradation of organic dye pollutant. *Int. J. Environ. Anal. Chem.* **100**, 225–240 (2020)
16. S.P. Kim, M.Y. Choi, H.C. Choi, Characterization and photocatalytic performance of SnO₂-CNT nanocomposites. *Appl. Surf. Sci.* **357**, 302–308 (2015)
17. S. Abbasi, M. Hasanpour, F. Ahmadpoor, M. Sillanpää, D. Dastan, A. Achour, Application of the statistical analysis methodology for photodegradation of methyl orange using a new nanocomposite containing modified TiO₂ semiconductor with SnO₂. *Int. J. Environ. Anal. Chem.* **101**, 208–224 (2021)
18. K. Shan, Z. Yi, X. Yin, D. Dastan, S. Dadkhah, B. Coates, H. Garmestani, Mixed conductivities of A-site deficient Y, Cr-doubly doped SrTiO₃ as novel dense diffusion barrier and temperature-independent limiting current oxygen sensors. *Adv. Powder Technol.* **31**, 4657–4664 (2020)
19. L. Sun, Z. Shi, L. Liang, S. Wei, H. Wang, D. Dastan, K. Sun, R. Fan, Layer-structured BaTiO₃/P(VDF-HFP) composites with concurrently improved dielectric permittivity and breakdown strength toward capacitive energystorage applications. *J. Mater. Chem. C* **8**, 10257–10265 (2020)
20. L. Sun, Zh. Shi, H. Wang, K. Zhang, D. Dastan, K. Sun, R. Fan, Ultrahigh discharge efficiency and improved energy density in rationally designed bilayer polyetherimide-BaTiO₃/P(VDF-HFP) composites. *J. Mater. Chem. A* **8**, 5750–5757 (2020)
21. W. Zhang, X. Zhu, L. Liang, P. Yin, P. Xie, D. Dastan, K. Sun, R. Fan, Z. Shi, Significantly enhanced dielectric permittivity and low loss in epoxy composites incorporating 3d W-WO₃/BaTiO₃ foams. *J. Mater. Sci.* **56**, 4254–4265 (2021)
22. D.A. Reddy, R. Ma, T.K. Kim, Efficient photocatalytic degradation of methyleneblue by heterostructured ZnO-RGO/RuO₂ nanocomposite under the simulated sunlight irradiation. *Ceram. Int.* **41**, 6999–7009 (2015)
23. M. Ahmad, E. Ahmed, Z.L. Hong, X.L. Jiao, T. Abbas, N.R. Khalid, Enhancement in visible light-responsive photocatalytic activity by embedding Cu-doped ZnO nanoparticles on multi-walled carbon nanotubes. *Appl. Surf. Sci.* **285**, 702–712 (2013)
24. S. Abbasi, Investigation of the enhancement and optimization of the photocatalytic activity of modified TiO₂ nanoparticles with SnO₂ nanoparticles using statistical method. *Mater. Res. Express* **5**, 066302 (2018)
25. S. Abbasi, Photocatalytic activity study of coated anatase-rutile titania nanoparticles with nanocrystalline tin dioxide based on the statistical analysis. *Environ. Monit. Assess.* **191**, 206–218 (2019)
26. D. Dastan, Nanostructured anatase titania thin films prepared by sol-gel dip coating technique. *J. Atomic Mol. Condens. Nano Phys.* **2**, 109–114 (2015)
27. D. Dastan, N.B. Chaure, Influence of surfactants on TiO₂ nanoparticles grown by sol-gel technique. *J. Mater. Mech. Manufact* **2**, 21–24 (2014)
28. S. Abbasi, S.M. Zebarjad, S.H.N. Baghban, Decorating and filling of multi-walled carbon nanotubes with TiO₂ nanoparticles via wet chemical method. *Engineering* **5**, 207–212 (2013)
29. S. Abbasi, S.M. Zebarjad, S.H.N. Baghban, A. Youssefi, Synthesis of TiO₂ nanoparticles and decorated multiwalled carbon nanotubes with various content of rutile titania. *Synth. React. Inorg. Met.-Org. Nano-Met. Chem.* **45**, 1539–1548 (2015)
30. N. Roozban, S. Abbasi, M. Ghazizadeh, Statistical analysis of the photocatalytic activity of decorated Multi-Walled carbon nanotubes with ZnO nanoparticles. *J. Mater. Sci.* **28**, 6047–6055 (2017)
31. S. Abbasi, Photocatalytic removal of methyl orange in suspension containing ZnO and SnO₂ nanoparticles and investigation the influence of effective variables on the process. *Iran. J. Health Environ.* **9**, 433–442 (2016)
32. S. Abbasi, Adsorption of dye organic pollutant using magnetic ZnO embedded on the surface of graphene oxide. *J. Inorg. Organometal. Polym. Mater.* **30**, 1924–1934 (2020)
33. S. Abbasi, M. Hasanpour, The effect of pH on the photocatalytic degradation of methyl orange using decorated ZnO nanoparticles with SnO₂ nanoparticles. *J. Mater. Sci.* **28**, 1307–1314 (2017)
34. H. Yuan, J. Xu, Preparation, characterization and photocatalytic activity of nanometer SnO₂. *Int. J. Chem. Eng. Appl* **3**, 214–246 (2010)
35. S. Abbasi, M.-S. Ekrami-Kakhki, M. Tahari, The influence of ZnO nanoparticles amount on the optimisation of photo degradation of methyl orange using decorated MWCNTs. *Prog. Ind. Ecol.* **13**, 3–15 (2019)
36. S. Abbasi, M. Hasanpour, Variation of the photocatalytic performance of decorated MWCNTs (MWCNTs-ZnO) with pH for photo degradation of methyl orange. *J. Mater. Sci.* **28**, 11846–11855 (2017)

37. M.-S. Ekrami-Kakhki, S. Abbasi, N. Farzaneh, Statistical analysis of the electrocatalytic activity of Pt nanoparticles supported on novel functionalized reduced graphene oxide-chitosan for methanol electrooxidation. *Electron. Mater. Lett.* **14**, 70–78 (2018)
38. M. Namvar-Mahboub, M. Pakizeh, Optimization of preparation conditions of polyamide thin film composite membrane for organic solvent nanofiltration. *Korean J. Chem. Eng.* **31**, 327–337 (2014)
39. M.-S. Ekrami-Kakhki, S. Abbasi, N. Farzaneh, Design of experiments methodology to investigate methanol electrooxidation on Pt nanoparticles supported novel functionalized reduced graphene oxide. *Anal. Bioanal. Electrochem.* **10**, 1548–1561 (2018)
40. A. Kazemi-Beydokhti, H.A. Namaghi, M.A.H. Asgarkhani, S.Z. Heris, Prediction of stability and thermal conductivity of SNO₂ nanofluid via statistical method and an artificial neural network. *Braz. J. Chem. Eng.* **32**, 903–917 (2015)
41. A. Ahmad, M.I. Ahmad, M. Younas, H. Khan, M.U.H. Shah, A comparative study of alkaline hydrolysis of ethyl acetate using design of experiments. *Iran. J. Chem. Chem. Eng.* **32**, 33–47 (2013)

Publisher's Note Springer Nature remains neutral with regard to jurisdictional claims in published maps and institutional affiliations.